Inorganic Chemistry

Article

pubs.acs.org/IC

Study of the Transition Metal Ordering in Layered $Na_xNi_{x/2}Mn_{1-x/2}O_2$ ($2/3 \leq x \leq 1$) and Consequences of Na/Li Exchange

Jordi Cabana,*[,†,‡,§] Natasha A. Chernova,[‖] Jie Xiao,[‖] Megan Roppolo,[‖] Kellie A. Aldi,[†] M. Stanley Whittingham,[‖] and Clare P. Grey*[,†,⊥]

[†]Department of Chemistry, Stony Brook University, Stony Brook, New York 11794-3400, United States

[‡]Environmental Energy Technologies Division, Lawrence Berkeley National Laboratory, Berkeley, California 94720, United States

[§]Department of Chemistry, University of Illinois at Chicago, Chicago, Illinois 60607-4306, United States

[‖]Institute for Materials Research, Binghamton University, Binghamton, New York 13902-6000, United States

[⊥]Department of Chemistry, University of Cambridge, Cambridge CB2 1EW, U.K.

Supporting Information

ABSTRACT: A series of layered oxides within the $Na_xNi_{ix/2}Mn_{1-x/2}O_2$ ($2/3 \leq x \leq 1$) system were synthesized by classical solid-state methodologies. A study of their long and short-range structure was undertaken by combining X-ray diffraction and NMR spectroscopy. A transition from P2 to O3 stacking was observed at $x > 0.8$ when samples were made at 900 °C, which was accompanied by disordering of ions in the transition metal layer. The magnetic properties of the materials were consistent with this picture of ordering, with all samples showing antiferromagnetic character. At $x = 2/3$, competition between a P2 and a P3 structure, with different degrees of transition metal ordering, was found depending on the synthesis temperature. Na/Li exchange led to structures with octahedral or tetrahedral coordination of the alkali metal, and Li/Ni crystallographic exchange in the resulting O3 phases. The transition from alkali metal prismatic coordination to octahedral/tetrahedral coordination involves $[TMO_6]_\infty$ layer shearing that induces some structural disorder through the formation of stacking faults.

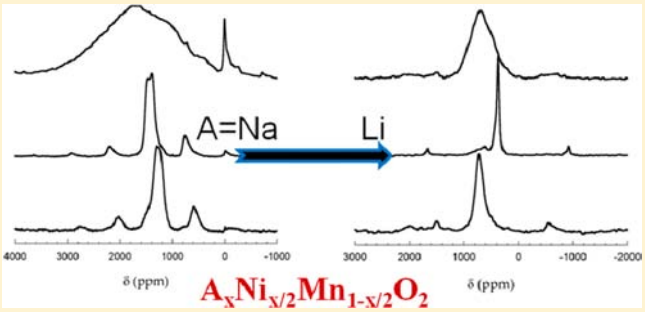

INTRODUCTION

The structural variability of alkali metal transition metal oxides with layered structures has been exhaustively documented over the past three decades.[1,2] The general structure of these compounds can be described as a closed packed array of oxide anions where the transition metal (TM) cations occupy the octahedral sites forming a pattern of alternating layers. The empty interlayer space is occupied by the alkali metal ions, the coordination of the site depending on the specific crystal structure. Despite the importance of the alkali metal in determining the specific framework arrangement, classifications were made early on that grouped compounds by the type of stacking of the $[TMO_6]_\infty$ slabs.[3] Labels were developed for the different classes of compounds whereby the coordination environment of the alkali metal was represented by O (octahedral), P (prismatic), etc., followed by the minimum number of $[TMO_6]_\infty$ layers that describe the periodic stacking. Thus, O3 corresponds to a crystal structure where the alkali metal resides in octahedral sites and the transition metal layers are staggered to form an ABCABC stacking. The occupancy of the alkali metal layer can affect the stacking sequence because of steric effects.[1,3] Water can also intercalate between $[MO_6]_\infty$ slabs, introducing additional complexity to this structural family. An example of this variability is the extremely rich $A_xMO_{2-y}\cdot H_2O$ (y represents anionic vacancies, A = alkali or alkaline earth) chemical space.[4,5]

Much of the attention directed at this broad family of compounds is justified by their properties, which make them intriguing from the point of view of their functionality and application. Although by no means a comprehensive list of all the technological fields in which layered alkali metal oxides find uses, phases with transition metals, such as Na_xCoO_2, are of interest in the context of battery,[6] thermoelectric,[7] and superconductivity[8] applications. The phases $Na_xNi_{x/2}Mn_{1-x/2}O_2$ ($2/3 \leq x \leq 1$), along with their ion exchanged Li counterparts, the subject of this paper, have received attention because of their excellent electrochemical performance when used as battery electrodes, whether for Li-ion[9−13] or Na-ion batteries.[14,15] The richness in properties is obviously linked to the tunability of their crystal-chemistry. For instance, soft chemistry ion exchange reactions can be performed to switch between alkali metals.[3,16,17] The effect of cation arrangements on physical properties has also been

Received: March 7, 2013
Published: July 24, 2013

   dx.doi.org/10.1021/ic400579w | Inorg. Chem. 2013, 52, 8540−8550

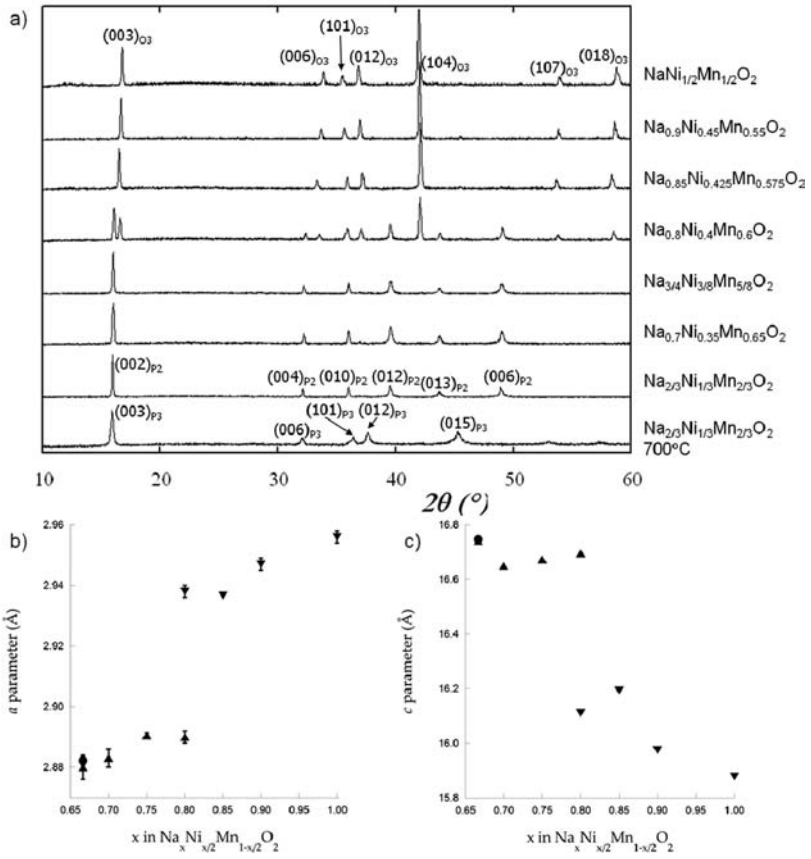

Figure 1. a) X-ray Diffraction (XRD) patterns of the $Na_xNi_{x/2}Mn_{1-x/2}O_2$ samples prepared in this study (see labels). Data is plotted in Cu Kα_1 radiation (λ = 1.5406 Å). Evolution of the (b) *a* and (c) *c* cell parameter vs *x*. The *c* parameter for the sample with P2 stacking has been multiplied by 1.5 to enable comparison with the samples with P3 and O3 stacking.

extensively documented.[18,19] Therefore, it is critical to develop sets of data that accurately describe the crystal-chemistry of these compounds at the atomic level.

Diffraction, using electron, X-ray or neutron sources, is the most commonly used tool to characterize composition and, especially, atomic arrangements in a crystalline framework. However, when more than one metal is introduced in the TM site, complexity can be introduced at the local level that is difficult to capture with this method. Nuclear magnetic resonance (NMR) spectroscopy can complement diffraction, providing insight into the interactions between the probe nucleus and its environment at distances of one to two chemical bonds. It can be performed on a variety of nuclei[20] with a collection of pulse sequences that interrogate different chemical and physical phenomena. When coupled with magic angle spinning, high spectral resolution can be achieved that has been extremely useful to characterize local ordering in compounds with various TMs.[21,22]

It is the goal of this study to produce a detailed picture of the crystal-chemistry of a variety of phases in the general $Na_xNi_{x/2}Mn_{1-x/2}O_2$ ($2/3 \leq x \leq 1$) system, with an emphasis on long and short-range ordering. X-ray diffraction and NMR data were combined with the measurement of magnetic properties, which are very sensitive to transition metal interactions. The structural changes that occur after exchanging Na by Li are also discussed.

EXPERIMENTAL SECTION

$Na_xNi_{x/2}Mn_{1-x/2}O_2$ ($2/3 \leq x < 1$) was prepared by firing pellets of Na_2CO_3 (99.5+ %, Aldrich), $Ni(OH)_2$ (99.3%, J.T. Baker) and Mn_2O_3 (99.9+ %, Aldrich) in stoichiometric proportions at 900 °C for 48 h in air, with intermediate grinding after 24 h. $NaNi_{1/2}Mn_{1/2}O_2$ and the low temperature phase of $Na_{2/3}Ni_{1/3}Mn_{2/3}O_2$ were prepared from Na_2CO_3 and a mixed hydroxide with appropriate Ni/Mn ratios. The hydroxides were prepared by slowly dripping a 50 mL aqueous solution of stoichiometric amounts of $Mn(NO_3)_2{\cdot}4H_2O$ (Fluka, >97%) and $Ni(NO_3)_2{\cdot}6H_2O$ (Aldrich, 99.999%) into 400 mL of a stirred solution of $LiOH{\cdot}H_2O$ (Sigma-Aldrich, >98%). The resulting brown precipitate was dried at 180 °C for 14 h, and mixed with Na_2CO_3 in stoichiometric proportions. The mixture was then pelletized and heat-treated at 700 °C for 24 h (x = 2/3) or at 800 °C for 15 + 15 h, with intermediate grinding (x = 1/2). All cooling steps were performed by quenching using liquid nitrogen. The oxides with x = 0.85, 0.9, and 1 were very moisture sensitive and, hence, were manipulated inside an Ar-filled glovebox.

Na/Li ion exchange reactions were performed in a molten salt eutectic of $LiNO_3$ and LiCl with ratio 88:12. The Li to Na ratio in the mixture was set to 10. The mixture was heated at 280 °C for 5 h in air. After ion exchange, the mixture was rinsed with distilled water and ethanol several times, and filtered to recover the powder. The whole process was repeated in order to drive the reaction to completion. The final powder was dried at 80 °C in air for one day.

Powder X-ray diffraction (XRD) patterns were obtained either with a Rigaku Miniflex powder diffractometer, which uses Cr Kα radiation (λ = 2.2909 Å), or a Scintag PAD V, with Cu Kα_1 radiation (λ = 1.5406 Å). All patterns are plotted in the latter radiation to allow comparison between data. $Na_xNi_{x/2}Mn_{1-x/2}O_2$ samples with x = 0.85, 0.9, and 1 were protected from moisture during the measurement by mixing them with silicone grease. The CELREF program[23] was used to

dx.doi.org/10.1021/ic400579w | Inorg. Chem. 2013, 52, 8540−8550

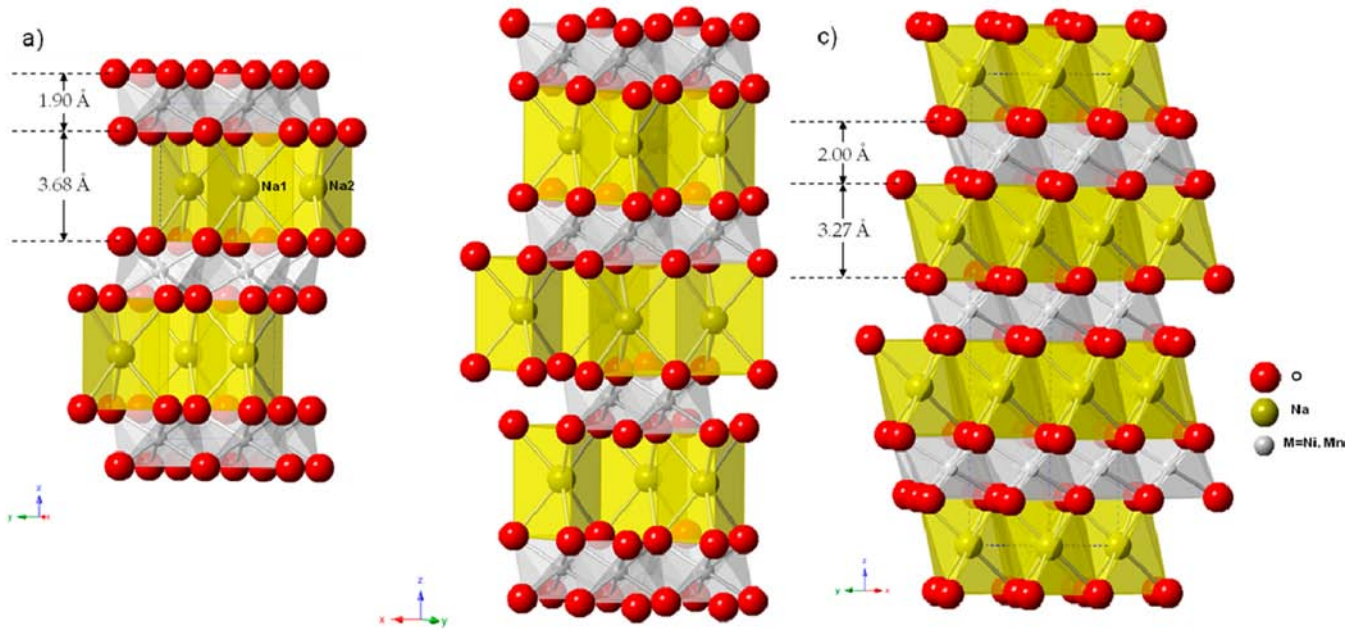

Figure 2. Representation of the structure for $Na_xNi_{x/2}Mn_{1-x/2}O_2$ crystallizing in (a) P2, (b) P3, and (c) O3 stacking. The two different interlayer spacings are indicated. Note that the Na sites are not completely populated for the P stackings.

refine the cell parameters of the obtained samples. Analysis and plotting of structural data in the literature[16,24,25] were carried out using CrystalMaker, a crystal and molecular structures program for Mac and Windows (CrystalMaker Software Ltd., Oxford, England; www.crystalmaker.com). The resulting values were devoid of statistical information and, thus, were used solely to establish qualitative trends in the discussion of the data reported here.

^{23}Na and ^{6}Li magic angle spinning nuclear magnetic resonance (MAS NMR) experiments were performed at 52.9 and 24.9 MHz, respectively, on a CMX-200 spectrometer in a field of 4.7 T using a 1.8 mm MAS probe at rotor spinning speeds (ν_r) of 38 kHz. A rotor synchronized spin−echo pulse sequence (90°−τ−180°−τ_1−acquisition) was used with typical 90° and 180° pulses of 1.6 and 3.2 μs, respectively, and recycle delays of 0.2 s. The spectra were referenced to 1 M solutions of ^{23}NaCl and ^{6}Li, respectively, by setting their signals at 0 ppm.

The magnetic properties were studied on Quantum Design MPMS and PPMS instruments. A SQUID magnetometer (Quantum Design MPMS XL-5) was used to measure the dc magnetic susceptibility ($\chi = M/H$, M is magnetization, H is applied magnetic field) of the samples from 350 to 2 K in a magnetic field of 1000 Oe. Field-cooled (FC) and zero-field-cooled (ZFC) magnetizations were measured over the same temperature range in a magnetic field of 10 Oe. FC data were measured by cooling the sample in the magnetic field. Before taking ZFC data, the remnant magnetic field was quenched to less than 3 mOe, the sample was cooled to 2 K, then the magnetic field was applied and the temperature dependence was measured while heating the sample. Magnetization curves were measured at 5 K in magnetic fields up to 5 T. In selected samples, the magnetization was measured up to 9 T at 5 K. The sample was zero-field cooled to 5 K before the magnetization data were taken.

RESULTS AND DISCUSSION

X-ray diffraction of $Na_xNi_{x/2}Mn_{1-x/2}O_2$ ($2/3 \leq x \leq 1$). Figure 1a shows the XRD patterns of all $Na_xNi_{x/2}Mn_{1-x/2}O_2$ prepared in this study. When the synthesis temperature was set at 900 °C, two structural domains were observed in this part of the phase diagram. At compositions $1 \leq x < 0.8$, the compounds crystallize in an O3 stacking (space group $R\bar{3}m$), whereas P2 stacking (space group $P6_3/mmc$) is observed at $0.8 < x \leq 2/3$. $Na_{0.8}Ni_{0.4}Mn_{0.6}O_2$ was systematically found to be a mixture of P2 and O3 stackings, even after several 24 h annealing cycles with intermediate grinding. At $x = 2/3$, two layer stacking types were found depending on the synthesis temperature: a P3 polytype (space group $R\bar{3}m$) was formed at 700 °C, and a P2 polytype at 900 °C.[12] Apart from changes related to the unit cell symmetry, the reflections of the P3 sample were found to be considerably larger than the P2. Formation of a P3 polytype was also observed when heating reaction mixtures with $x = 1$ at 700 °C (data not shown). However, this phase was accompanied by significant amounts of NiO, leading to the conclusion that the Ni/Mn, and, consequently, Na/(Ni + Mn) ratio in the layered sodium-containing phase were well below 1.

The cell parameters obtained after indexing the patterns are shown in Figure 1b and c. Note that the c parameter corresponding to the samples showing P2 stacking was multiplied by a factor of 3/2 so as to enable comparisons with the O3 and P3 polytypes. Both the size of the cell in the ab plane (Figure 1b) and the distance between $[TMO_6]_\infty$ (TM = Ni, Mn) slabs (Figure 1c) in $Na_{2/3}Ni_{1/3}Mn_{2/3}O_2$ are independent of the temperature of synthesis, as expected from the fact that the composition and the coordination of the Na site are the same (Figures 2a and b). A largely monotonic increase in a parameter with Na content (i.e., x), together with a decrease in c, occurs in the samples crystallizing with the same polytype. The expansion of the ab plane is ascribed to the introduction of Ni^{2+} in the transition metal layer at the expense of the smaller Mn^{4+} ion (ionic radii = 0.69 vs 0.53 Å, respectively),[26] as well as to a steric effect arising from the increasing occupancy of the Na^+ sites. Conversely, the contraction occurring perpendicular to the layers, especially for the O3 polytypes, is most likely due to the increased presence of Na^+ ions between $[TMO_6]_\infty$ layers. The alkali ions

dx.doi.org/10.1021/ic400579w | Inorg. Chem. 2013, 52, 8540−8550

Table 1. Na−O and Na−O−Transition Metal (TM) Bonding in P2-$Na_{2/3}Ni_{1/3}Mn_{2/3}O_2$ (Space Group $P63/mmc$), O3-$NaNi_{1/2}Mn_{1/2}O_2$ (Space Group $R\bar{3}m$), and P3-$Na_{2/3}Ni_{1/3}Mn_{2/3}O_2$ (Space Group $R\bar{3}m$)[a]

phase	site	Na−O distance (Å)	TM	no.	Na−O−TM angle (deg)	Na−TM distance (Å)	no. Na−O−TM
P2−$Na_{2/3}Ni_{1/3}Mn_{2/3}O_2$[b]	Na1	2.48	Mn/Ni	2	77.7	2.80	6
				12	131	4.01	12
	Na2			6	94.4	3.25	12
				6	162	4.35	6
P3−$Na_{2/3}Ni_{1/3}Mn_{2/3}O_2$[c]	Na1	2.53		1	79.1	2.88	3
				6	132	4.08	6
		2.41		3	93.7	3.18	6
				3	164	4.30	3
O3-$NaNi_{1/2}Mn_{1/2}O_2$[d]	Na1	2.37		6	92.5	3.16	12
				6	167	4.32	6

[a]The values were extracted from the structures reported by others in the literature after refinement of powder diffraction data,[16,24,25] using CrystalMaker, a crystal and molecular structures program for Mac and Windows (CrystalMaker Software Ltd, Oxford, England; www.crystalmaker.com). They are thus devoid of statistical information. [b]d(Mn−O) = d(Ni−O) = 1.92 Å; $d(O-O)_{c,slabNa}$ = 3.68 Å; $d(O-O)_{c,slabMn/Ni}$ = 1.90 Å. [c]d(Mn−O) = d(Ni−O) = 1.93 Å; $d(O-O)_{c,slabNa}$ = 3.65 Å; $d(O-O)_{c,slabMn/Ni}$ = 1.94 Å. [d]d(Mn−O) = d(Ni−O) = 1.98 Å; $d(O-O)_{c,slabNa}$ = 3.27 Å; $d(O-O)_{c,slabMn/Ni}$ = 2.00 Å.

screen their negative charges, thereby pinning them closer together.

As the Na coordination is changed from pyramidal to octahedral, at around x = 0.8, positive and negative discontinuities were found in the trends of the a and c parameters, respectively. The negative discontinuity in the c parameter is assigned to the gliding of the $[TMO_6]_\infty$ layers. The change from being aligned along the c axis (P) to being staggered (O) reduces the repulsion between the anions, allowing the layers to move closer, driven by the electrostatic interactions with the Na^+ ions (Figure 2). Indeed, analysis of other structural information available in the literature for both P2-$Na_{2/3}Ni_{1/3}Mn_{2/3}O_2$[16] and O3-$NaNi_{1/2}Mn_{1/2}O_2$[24,25] (Table 1) revealed a contraction of the $[TMO_6]_\infty$ interlayer distance from 3.68 Å in the P2 phase to 3.25 Å in the O3. It is worth noting that the distances between $[NaO_6]_\infty$ layers were found to be 1.90 and 2.00 Å for P2 and O3, respectively (Figure 2a and c). This increase is another expression of the steric effect of substituting Mn^{4+} by Ni^{2+}, which pushes the O^{2-} further away, yet it is insufficient to drive an overall expansion along the c direction. The positive discontinuity in a parameter with the change in stacking from P to O could be a reflection of bonding changes in the transition metal layer. The TM−O (TM = Ni, Mn) distances for P2-$Na_{2/3}Ni_{1/3}Mn_{2/3}O_2$ and O3-$NaNi_{1/2}Mn_{1/2}O_2$ resulting from the analysis of structural data extracted reported by others are 1.92 and 1.98 Å, respectively (Table 1).[16,24,25] These distances are predicted to be 1.98 and 2.01 Å, respectively, from the weighted average of the ionic radii of all the ions,[26] suggesting that some level of compression of the Ni−O bonds exists in the P2 compound. A similar situation was found for $Li[Li_{1/3}Mn_{2/3}]O_2$ (Li_2MnO_3), which has a similar cationic arrangement in the transition metal layer (see below).[27] Compression in the $Li-O^{2-}$ distances (2.05 and 2.07 Å) was found for sites within the Mn layer compared to the values predicted by the sum of the ionic radii (2.16 Å). In contrast, the $Mn^{4+}-O^{2-}$ distances (1.90 and 1.92 Å) were found to be very close to the predicted value (1.93 Å). Increased Na/vacancy or Ni/Mn ordering could favor cooperative bond relaxation within $[MnO_6]_6$ honeycombs in a $\sqrt{3}a \times \sqrt{3}a$-type ordering arrangement, forcing Ni−O bonds to be shorter.

Overall, the XRD results largely follow what was previously reported for $Na_xNi_{x/2}Ti_{1-x/2}O_2$.[28] However, since Ni and Mn have similar X-ray scattering power, it is not possible to extract any insight into the existence of atomic ordering in these layered structures, the objective of this work. Thus, a study of these short-range interactions was undertaken using magnetic susceptibility and NMR data, which is reported below.

Magnetic Measurements. The temperature dependence of the magnetic susceptibilities measured at 1000 Oe (Figure 3a) showed peaks typical of antiferromagnetic ordering for all

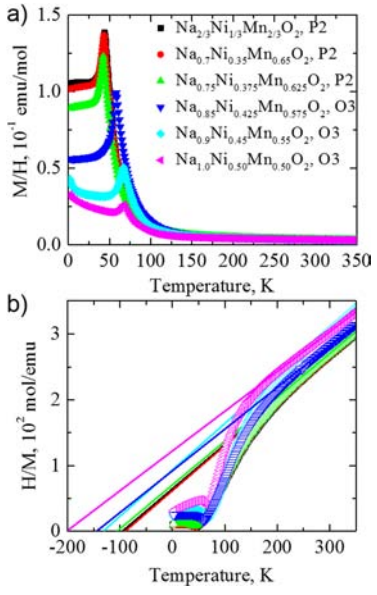

Figure 3. (a) Temperature dependences of the magnetic susceptibility of the $Na_xNi_{x/2}Mn_{1-x/2}O_2$ samples and (b) their reciprocals fitted to the Curie−Weiss law.

the compositions. The Néel temperature, T_N, defined as a maximum of $d(\chi T)/dT$, shifted from 64 to 56 K as the Na content decreased from x = 1 to x = 0.85. It further decreased to 41−43 K in the P2 phases, but a more modest dependence with composition was found (Table 2). It is proposed that this transition temperature is dependent on the interslab magnetic exchange, which will be strengthened by the decrease in interslab distance with Ni content (Figures 1 and 2). This decrease is more modest in the P2 phases, consistent with the lower variability between them. The magnetic susceptibility

dx.doi.org/10.1021/ic400579w | Inorg. Chem. 2013, 52, 8540−8550

Table 2. Magnetic Parameters of $Na_xNi_{x/2}Mn_{1-x/2}O_2$

polytype	x	T_N (K)	H_M (5 K, T)	C (emu/K mol)	Θ (K)	μ_{exp}, μ_B	μ_{theor}, μ_B	M_{s_exp} (μ_B)	M_{s_theor} (μ_B)
O3	1.0	64.0	2.8	1.604(8)	−186.8(7)	3.58	3.39	0.45	0.500
	0.9	64.0	1.4	1.450(4)	−142.9(6)	3.41	3.44	0.63	0.750
	0.85	56.0	1.2	1.570(2)	−144.4(2)	3.55	3.47	0.81	0.875
P2	0.75	41.0	1.8	1.498(3)	−111.4(3)	3.43	3.52	1.07	1.125
	0.7	41.5	1.6	1.459(2)	−89.8(2)	3.42	3.54	1.16	1.250
	2/3	42.5	1.6	1.477(2)	−95.3(3)	3.44	3.56	1.25	1.333

approached a Curie−Weiss behavior at high temperature so that linear fits of the reciprocal susceptibility were possible from 300 to 350 K (Figure 3b). The resulting values of the molar Curie constant, C, and Curie−Weiss temperature, Θ, along with the effective magnetic moment, $\mu_{exp} = (8C)^{1/2}$, are presented in Table 2. Although the effective magnetic moments showed overall agreement with μ_{theor} values calculated assuming Ni^{2+} (S = 1) and Mn^{4+} (S = 3/2), the linear decrease expected with increasing Ni^{2+} content was not clearly observed. The O3 phases x = 1 and 0.85 showed anomalously large μ_{exp} values with respect to theoretical (3.58 and 3.55 vs 3.39 and 3.47 μ_B, respectively). This discrepancy was attributed to the moisture sensitivity of these samples, as intercalation of water between the transition metal layers in Na_xMO_2 (M = Co, Mn, Ni) is well-known to lead to changes in magnetic properties.[8] The P2 phases show systematically lower than expected Curie constants indicating that the Curie−Weiss regime may not be fully achieved at 300−350 K. The Curie−Weiss temperatures were negative in all the compounds, indicating antiferromagnetic exchange. The increase in the absolute temperature value with Ni^{2+} content implied strengthening of the magnetic exchange within the transition metal slabs. The corresponding increase in a lattice parameter (Figure 1) should weaken it if their composition was the same. Therefore, this behavior was dominated by the increase in the number of antiferromagnetic Mn^{4+}−O−Ni^{2+} contacts with Ni^{2+} content, in agreement with the Goodenough−Kanamori rules.[29,30]

The magnetic susceptibilities measured at 10 Oe under FC and ZFC conditions showed a single maximum for the O3 samples (Figure 4). Minor FC-ZFC deviations were noticed below T_N, again consistent with antiferromagnetic ordering. The ZFC curves of the samples with P2 stacking peaked at T_N. In contrast, the FC susceptibility sharply increased at the same temperatures, resulting in a departure between curves typical of net magnetic moment formation. A similar sustained increase in FC susceptibility with temperature was also observed at 20 Oe for P2, x = 2/3, but a progressive change in the curves was observed as the field was increased (data not shown), so that a maximum at 43 K developed at 1000 Oe (Figure 3). Additional, subtle features were observed between 20 and 30 K in both FC and ZFC curves of x = 2/3 and 0.7; their nature is currently unclear.

The magnetization curves measured at 5 K show virtually no hysteresis at small fields for all compositions (Figure 5), an indication of the absence of Ni^{2+}/Na^+ interlayer exchange[31] expected from the radius mismatch between the two ions[26] and in contrast to results typically observed for related lithiated materials.[31] The change in the magnetization slope noticed for all compounds at fields that vary from 10 to 30 kOe was ascribed to the occurrence of a metamagnetic (spin-flip) transition. The O3 phases showed strong hysteresis around the metamagnetic transition field, H_M, where the magnetization and demagnetization curves noticeably departed from each other.

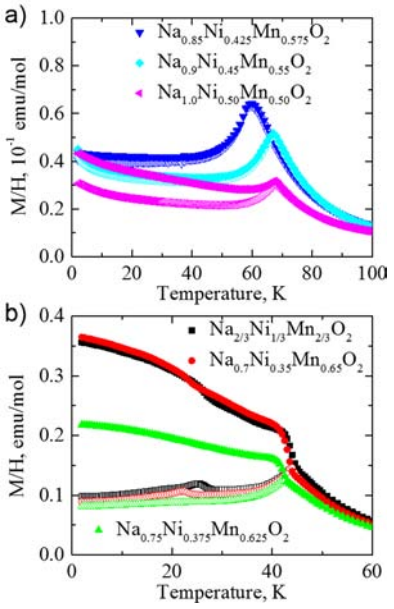

Figure 4. Temperature dependences of field-cooled (solid symbols) and zero-field-cooled (open symbols) magnetic susceptibilities of (a) O3- and (b) P2-$Na_xNi_{x/2}Mn_{1-x/2}O_2$ samples.

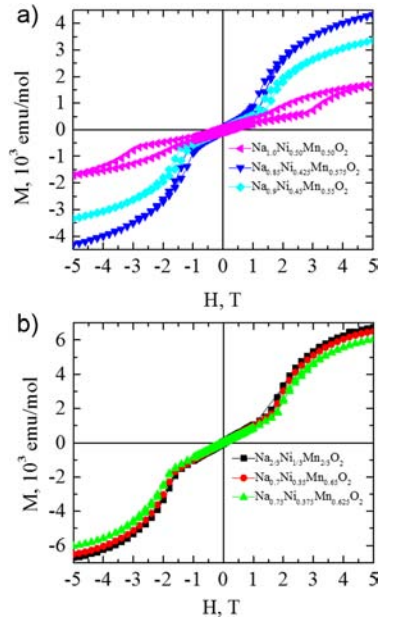

Figure 5. Magnetization curves at 5 K of (a) O3- and b) P2-$Na_xNi_{x/2}Mn_{1-x/2}O_2$ samples.

The magnitude of both H_M and the hysteresis increased with Na content (Table 2). In contrast, the P2 phases did not show any hysteresis around the metamagnetic transition, which was

dx.doi.org/10.1021/ic400579w | Inorg. Chem. 2013, 52, 8540−8550

found to be less dependent upon composition than for the O3 phases. The saturation magnetization values determined at 9 T (Table 2) were consistent with a model assuming antiferromagnetic alignment of Ni^{2+} ($M_s = 2\ \mu_B$) and Mn^{4+} spins ($M_s = 3\ \mu_B$) within the $[TMO_6]_\infty$ layer. As a result, each layer possesses a net magnetic moment that decreases with Ni content. At small fields, this net magnetic moment alternates from layer to layer, along the c axis, creating an overall antiferromagnetic alignment. In turn, a slight canting of the magnetic moments seems to take place either within or between the $[TMO_6]_\infty$ layers in the P2 framework, causing a net magnetic moment up to 20 Oe field which is in agreement with earlier work.[32] An increase of the magnetic field suppresses the canting, so that antiferromagnetic order is observed above 1000 Oe and until the metamagnetic transition. At the metamagnetic transition, the magnetic moments of the $[TMO_6]_\infty$ layers flip from antiferromagnetic to ferromagnetic arrangement, inducing overall ferrimagnetic ordering. This model gives excellent agreement between observed and calculated values of the saturation magnetization (Table 2). The hysteresis of the magnetization observed in the O3 phases probably results from the smaller interlayer distance, which makes the spin-flip transition more difficult. The absence of a regular dependence of H_M with interlayer distance reflects that it is also affected, although in the opposite way, by the net increase in magnetic moment of the layer with the interlayer distance.

The magnetic transitions are significantly broadened in the O3 compared to the P2 phases (Figures 3 and 4), indicating higher degree of structural ordering in the latter. The temperature dependence of the heat capacity was measured for $x = 1$, O3, and $x = 2/3$, P2 (Figure 6). A sharp λ-feature

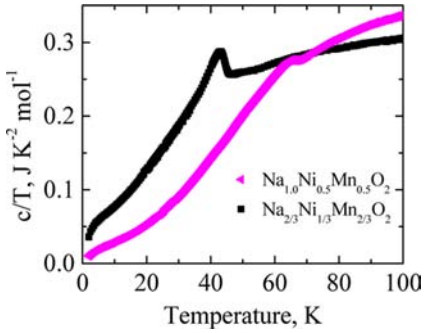

Figure 6. Temperature dependence of the heat capacity of $NaNi_{0.5}Mn_{0.5}O_2$ and $Na_{2/3}Ni_{1/3}Mn_{2/3}O_2$.

would be predicted for a true magnetic ordering transition. The data revealed a very broad feature for $x = 1$, O3, at 65 K, compared to a well-defined, albeit not very sharp, λ-feature at 43 K for $x = 2/3$, P2.

Li Ion Exchange Reactions. Exchange of Na for Li was carried out by multiple 5 h treatments in molten LiCl-$LiNO_3$. Differences in the rate of ion exchange were noticed among samples of different polytypes. In general, exchange was apparently complete in 10 h for all samples crystallizing in the P2 and P3 polytypes, whereas some intermediate phases were observed for some of the O3 samples even after 35 h. This difference in rate of exchange is likely an indication of the mobility of Na^+ ions within the layered framework of both polytypes, driven by the larger number of vacancies and interlayer spacing in the P versus the O phases, as well as the existence of wide rectangular bottlenecks between prisms.[35,36] Exchange was completed in 10 h for O3-$NaNi_{1/2}Mn_{1/2}O_2$ made from a hydroxide precursor, which indicates that powder microstructure also plays a critical role in the rate of the reaction. Because of its technological interest as Li-ion battery electrode,[11] the resulting $LiNi_{1/2}Mn_{1/2}O_2$ will be the object of a separate detailed study.

Figure 7 shows the XRD patterns collected at different steps of the reaction for O3−$Na_{0.9}Ni_{0.45}Mn_{0.55}O_2$. No initial Na phase

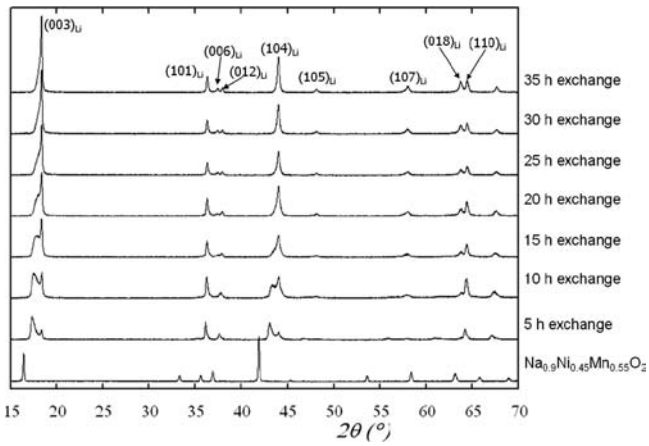

Figure 7. X-ray diffraction (XRD) patterns of samples obtained during the Na/Li exchange of $Na_{0.9}Ni_{0.45}Mn_{0.55}O_2$ at different time intervals, as indicated. Data is plotted in Cu Kα_1 radiation (λ = 1.5406 Å).

was observed after only 5 h, but an intermediate phase was found alongside the final lithiated product. While the width of the peaks precludes peak indexing, this intermediate appeared to show a layered structure that resembles the final product, albeit with larger unit cell dimensions. It was assigned to a phase with an intermediate content of Na and Li that reflected an incomplete reaction. As more 5 h steps were completed, further Na/Li exchange occurred within the intermediate, as reflected by the progressive shift of its peaks toward lower angles, an indication of lattice shrinkage because of the smaller ionic radius of Li compared to Na.[26] The intermediate simultaneously disappeared at the expense of the final phase, yet a shoulder at lower angles on the (003) reflection at 18.3°, 2θ, persisted even after 30 h, indicating that the reaction was still not complete. No changes in cell parameter were observed for the final phase during the two-phase coexistence. Nonetheless, the (018) and (110) reflections, at 63.7° and 64.4°, 2θ, became increasingly resolved with ion exchange time. An increase in the ratio of the (003) over the (104) reflection, at 18.4° and 44.0°, 2θ, simultaneously took place. Such evolution could be an indication that the ion exchange process induced structural defects in the Li-containing phase, which were eliminated as the reaction got close to completion.

X-ray Diffraction of $Li_xNi_{x/2}Mn_{1-x/2}O_2$ ($2/3 \le x \le 1$) Phases. The exchange reaction of phases with O3 and P3 stacking resulted in Li phases with an O3 structure (hexagonal, $R\bar{3}m$ space group, Figure 8a), consistent with previous reports.[11,16,17,24,25,33] A different stacking was obtained by ion exchange from P2 phases. The existence of two peaks at ~65° and 66°, 2θ, in all samples was indicative of a T2 stacking in which Li^+ ions are located in tetrahedral sites between the transition metal layers.[17] These two peaks correspond, respectively, to the (111) and (110) reflections of an

dx.doi.org/10.1021/ic400579w | Inorg. Chem. 2013, 52, 8540−8550

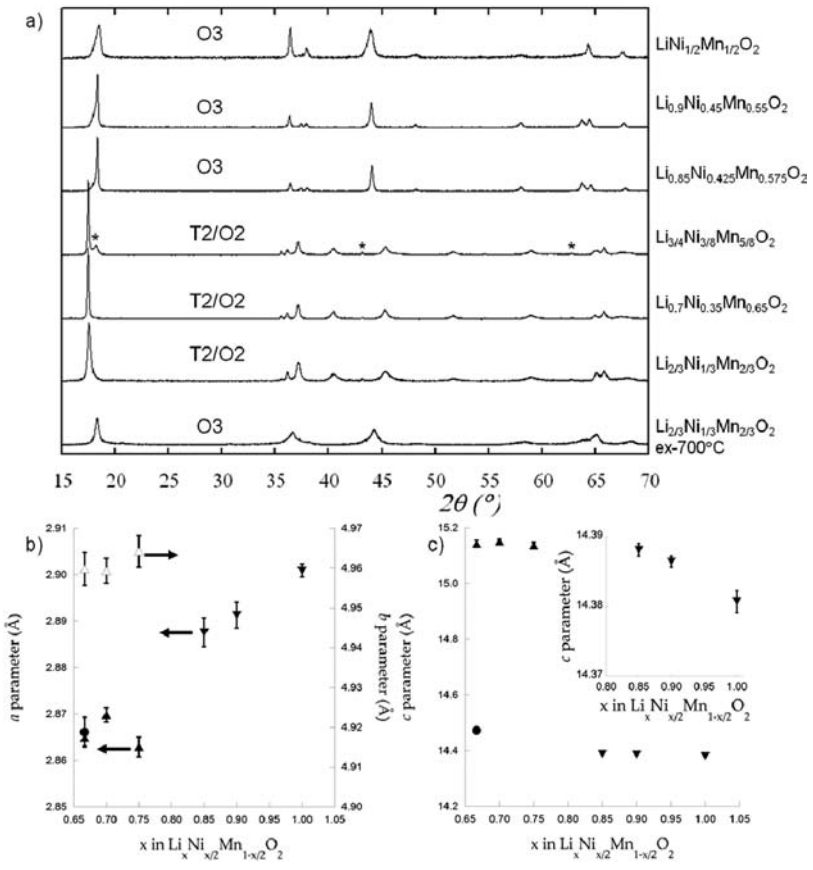

Figure 8. (a) X-ray diffraction (XRD) patterns of the $Li_xNi_{x/2}Mn_{1-x/2}O_2$ samples prepared in this study (see labels). Data is plotted in Cu Kα_1 radiation (λ = 1.5406 Å). Evolution of the (b) *a*, *b* ("*b*" only for samples crystallizing in an orthorhombic cell, see text for details) and (c) *c* cell parameter *vs x*. The *c* parameter for the sample with T2/O2 stacking has been multiplied by 1.5 to enable comparison with the samples with P3 and O3 stacking. The inset in (c) is a zoom-in of the area corresponding to samples with $x > 0.8$.

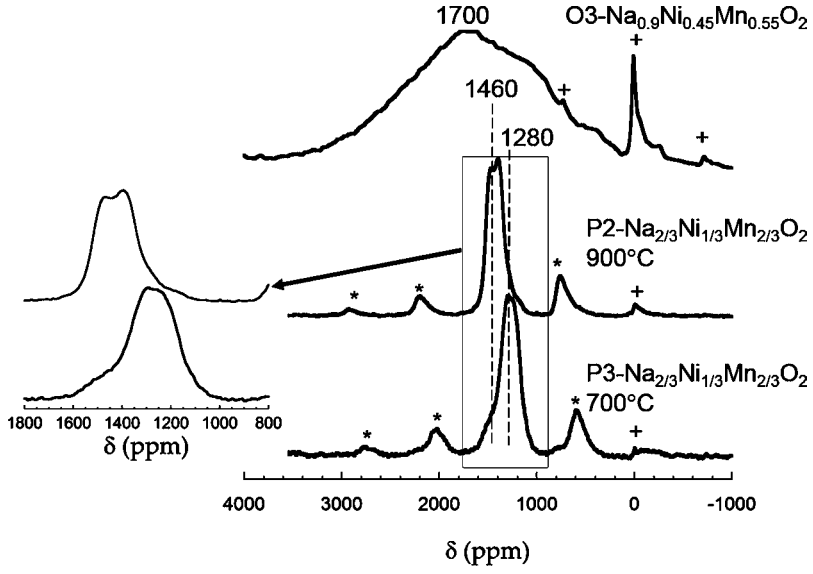

Figure 9. ^{23}Na MAS NMR spectra of selected $Li_xNi_{x/2}Mn_{1-x/2}O_2$, as labeled, acquired at a spinning speed of 38 kHz, normalized to the amount of sample in the rotor. The "*" indicates the spinning sidebands for the main centerband. The peaks marked with "+" correspond to the isotropic resonance for a diamagnetic impurity, most likely Na_2CO_3, at around 0 ppm, and its spinning sidebands.

orthorhombic unit cell (*Cmca* space group). Their intensity ratio, (111)/(110), is an indication of the competition between T2 and O2 stacking (hexagonal, $P6_3mc$ space group).[33] The ratio was the highest for x = 0.7, indicating that this sample is the closest to the ideal T2 structure, whereas the other two likely contained domains of O2 or O2 stacking faults.[34] Additional peaks that could not be indexed with this orthorhombic cell were observed at 18.2°, 43.1°, and 62.8°,

dx.doi.org/10.1021/ic400579w | *Inorg. Chem.* 2013, 52, 8540−8550

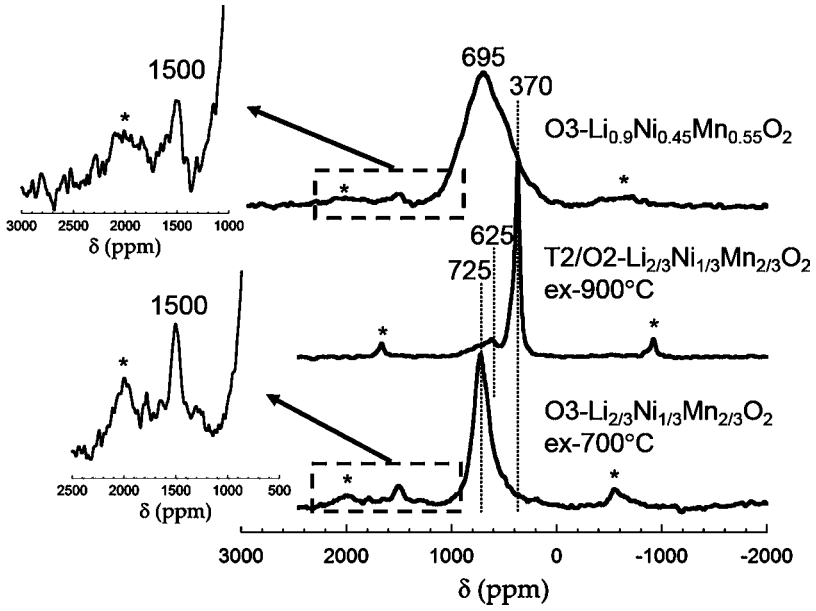

Figure 10. ^{6}Li MAS NMR spectra of selected $Li_xNi_{x/2}Mn_{1-x/2}O_2$, as labeled, acquired at a spinning speed of 38 kHz, normalized to the amount of sample in the rotor. The "*" indicates the spinning sidebands for the main centerband.

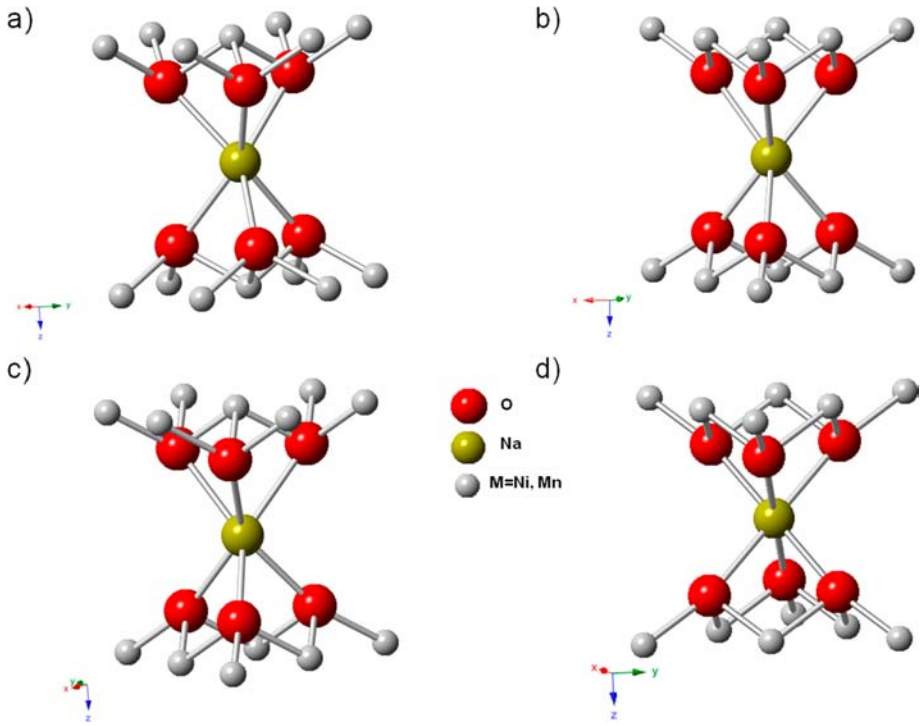

Figure 11. Local environment of Na in $Na_xNi_{x/2}Mn_{1-x/2}O_2$ crystallizing in (a, b) P2 (Na1 and Na2, respectively), (c) P3, and (d) O3 stacking.

2θ, (see "*" in Figure 8a) especially for sample $x = 3/4$. Similar peaks have been reported by others,[10,13,16,35] but no satisfactory explanation for their presence is available. Their intensity was shown to stay unaffected even after repeated ion exchange treatments.

The XRD patterns were indexed in order to calculate the corresponding cell parameters (Figure 8b and c). As in Figure 1, a 3/2 correction factor was applied to the c parameter values of the T2/O2 phases to enable comparison with the O3 samples. Considerable scatter and larger errors was observed in the values at $x < 0.8$. These effects were a reflection of the notable width of the reflections for $x = 2/3$, O3, and are an indication of the competition between O2 and T2 stacking, which were not accounted for by the indexing software. In general, the same trends were observed for the Li as for the Na phases with transition metal content, i.e., increase in the dimension of the ab plane and decrease in the c direction. The close-to-linear behavior by the O3 phases was consistent with the existence of a solid solution. Contrary to what was discussed above for the Na phases, the c parameter of the $x = 2/3$, T2/O2 phase was higher than for the O3 phase.[26] To evaluate whether changes in cationic ordering could be at the

dx.doi.org/10.1021/ic400579w | Inorg. Chem. 2013, 52, 8540−8550

origin of these observations, and since refinement of Li and Ni/Mn contents and positions in their respective sites is not possible using XRD data, these compounds were also analyzed by NMR.

MAS NMR of $A_xNi_{x/2}Mn_{1-ix/2}O_2$ (A = Li, Na, 2/3 ≤ x ≤ 1) phases. The ^{23}Na and ^{6}Li MAS NMR spectra corresponding to $x = 0.9$ and the two forms observed at $x = 2/3$ for A = Na and Li are shown in Figures 9 and 10, respectively. Very subtle shifts to lower frequencies with no change in line shape were found between different compositions of the same polytype (see Supporting Information Figure S1). The NMR shifts were predictably large and nonzero in both the ^{23}Na and ^{6}Li spectra because of the existence of A-X-TM (where A = Li, Na, X = anion, TM = Ni, Mn) hyperfine contacts with paramagnetic centers.[21] These dipolar interactions also lead to considerable static line broadening, which, under MAS, results in broad sideband manifolds. Sharp peaks were observed at around 0 ppm, especially in some ^{23}Na NMR spectra, which are ascribed to diamagnetic impurity phases such as Na_2CO_3. These impurities were not detected by XRD because they were likely present in very small amounts.

^{23}Na is a high magnetogyric ratio, γ, quadrupolar nucleus with $I = 3/2$. Quadrupolar interactions between the ^{23}Na nuclei and the surrounding electrical field gradient result in satellite transitions that are broadened to first order by the quadrupolar interaction. This interaction is partially averaged by MAS. In contrast, the central transition is only affected to second-order by the quadrupolar interaction, leading to complex and asymmetric line broadening even under MAS.[36,37] Well-resolved lineshapes were observed for the P polytypes, but with distinct differences between P2- and P3-$Na_{2/3}Ni_{1/3}Mn_{2/3}O_2$ (see zoom in Figure 9). Attempts were made to simulate these spectra (see Supporting Information), but, in the absence of data at more than one field, it was not possible to achieve unambiguous fits. Nonetheless, the spectra indicate that only a limited subset of local environments was present. No resolved isotropic resonances and spinning sidebands could be detected in the ^{23}Na MAS NMR spectra of the O3 phase (at $x \geq 0.85$), which were ascribed to a combination of the large line dipolar broadening, and the large range and breadth of the (presumably multiple) isotropic resonances in this sample (see below). The largest shifts, as estimated from the center of gravity of the resonances, were observed for the O3 polytypes, followed by the P2 and the P3 polytypes. The jump is most likely dominated by the discontinuities in Na−O−TM bond distances and angles caused by the different coordination environments. The most efficient overlaps are predicted to occur in an O3 structure because it results in the shortest Na−O distances, as well as more Na−O-TM contacts closest to the ideal 90 and 180° (Table 1 and Figure 11).[21] The more subtle shift of the center of gravity between the P3 and P2 phases (1280 vs 1460 ppm, respectively) is likely the result of complex interactions that will be discussed below.

General similarities were found in the trends of the ^{6}Li spectra after Na/Li exchange, the ^{6}Li signals being much broader for $x = 0.9$ than for either $x = 2/3$ sample (Figure 10). The very broad ^{6}Li resonance in the spectrum of $x = 0.9$, O3 was centered around 695 ppm, consistent with data reported for $x = 1$.[11,25] In turn, a much sharper asymmetric resonance centered at 725 ppm was found in the spectrum of $x = 2/3$, O3, consistent with only a few local environments. The noticeably larger Mn^{4+}/Ni^{2+} ratio in $x = 2/3$ with respect to $x = 0.9$ (2 and 0.8, respectively) should lead to differences in Li NMR shifts.[38] In practice, the centers of gravity for both samples were similar. The proximity in center of gravity may reflect the larger interlayer spacing for Li in $x = 2/3$ compared to 0.9 (Figure 8c), which consequently results in longer Li−O−Mn/Ni lengths that weaken the Fermi contact and compensate for the differences in Mn^{4+}/Ni^{2+} ratio.

A small, broad resonance was observed at 1500 ppm in the spectra of both O3 samples, which is assigned to Li in a honeycomb-like arrangement of manganese ions (i.e., 6 Mn nearest neighbors) within the transition metal layer, as is found $Li[Li_{1/3}Mn_{2/3}]O_2$ (Li_2MnO_3).[39,40] It reflects the existence of crystallographic Li/Ni exchange in the layered oxides, as occurs when $LiNi_{1/2}Mn_{1/2}O_2$ is made directly in the Li form.[41−43] Since no evidence of Na/Ni exchange was found in the Na precursors, the formation of the Li/Ni exchange must have taken place during ion exchange. Such exchange is known to be absent for $x = 1$ when made by ion exchange of O3-$NaNi_{1/2}Mn_{1/2}O_2$ in the same conditions,[11,25] but it can be introduced upon heating above 500 °C.[44] Our data strongly suggest that it can occur at even lower temperatures (280 °C in this study) when vacancies exist in the alkali metal layer. Evidence of shuttling of Ni^{2+} ions between the alkali and transition metal layer in the presence of vacancies is available in the literature.[45]

The ^{6}Li MAS NMR spectrum of T2/O2-$Li_{2/3}Ni_{1/3}Mn_{2/3}O_2$ showed notable differences as compared to its O3 counterpart. The narrow resonance at 370 ppm that dominates the spectrum is accompanied by a shoulder at 430 ppm and several broad, but small resonances with lower intensity between 600 and 1000 ppm. The much lower value of the main resonance for the T2/O2 stacking with respect to the O3 at the same Ni and Mn content was ascribed to the decrease in Li−O−Mn contacts when the coordination is changed from octahedral to tetrahedral, as well as a reduced orbital overlap between Li, O and Ni/Mn with increasing interlayer spacing (Figure 8).

Cationic Ordering in the Transition Metal Layers of $A_xNi_{x/2}Mn_{1-x/2}O_2$ (A = Li, Na, 2/3 ≤ x ≤ 1). Earlier analyses of powder neutron diffraction data for $x = 2/3$, P2 and P3 revealed superlattice reflections that were ascribed to the formation of a $\sqrt{3}a \times \sqrt{3}a$-type superlattice because of Ni/Mn ordering.[24] Asymmetry in the superlattice reflections in the P3 polytype was proposed to stem from the lack of registry between layers, possibly due to stacking faults. A more recent analysis of neutron powder diffraction and pair distribution function (PDF) data for $x = 0.5$, O3 revealed a trend toward short-range correlations within a largely disordered structure that favored the formation Ni and Mn pairs in a zigzag-like manner.[25] These observations are largely consistent with the existence of better defined (albeit not perfectly sharp) magnetic transitions of $x = 2/3$ P2 versus O3 and a λ-feature in the heat capacity observed for $x = 2/3$. The ordering trends were found to be largely preserved in the neutron diffraction data after Na/Li exchange.[24,25] In a completely ordered structure, the resulting small number of generally well-resolved NMR peaks can be traced back to the number of crystallographic sites and, in this particular case, discrete ratios of Ni^{2+} and Mn^{4+} ions in the Li or Na environment. A large collection of resonances at different frequencies will appear when disorder increases, resulting in an overall decrease in spectral resolution. Thus, the noticeably larger resonance width observed in the ^{23}Na and ^{6}Li MAS NMR spectra of the $x = 0.9$ vs the $x = 2/3$ phases

dx.doi.org/10.1021/ic400579w | Inorg. Chem. 2013, 52, 8540−8550

(Figures 9 and 10) is also indicative of a large degree of Ni/Mn disorder in the former.

Complete cationic ordering in P2-$Na_{2/3}Ni_{1/3}Mn_{2/3}O_2$ leads to splitting of the 2 crystallographic sites expected for Na in the ideal structure (Table 1 and Figures 2 and 11a, b).[24] Simulations of the ^{23}Na MAS NMR spectrum of P2-$Na_{2/3}Ni_{1/3}Mn_{2/3}O_2$ using a single line did not yield a satisfactory fit (Supporting Information Figure S2 and Table S1), suggesting the existence of multiple Na environments. Lack of signal resolution precluded the determination of their precise number, and, thus, an assessment of the extent and type of Ni/Mn order. It is also possible that the spectrum was affected by ion motion on the time scale of the NMR signal, which affects the width of the signals and can even lead to their complete averaging.[46] Na^+ mobility was reported to occur in P2-$Na_{2/3}Ni_{1/3}Ti_{2/3}O_2$ above approximately 270K from NMR data,[47] with motional narrowing shown to continue up to 480K, indicating that signal averaging was not complete at low temperatures. The change in stacking from P2 to P3 in $Na_{2/3}Ni_{1/3}Mn_{2/3}O_2$ is due to a shearing of the oxygen layers that increases the symmetry of the cell[1] and reduces the number of Na crystallographic positions from 2 to 1 (Figure 11, Table 1).[24] Again, attempts at simulating the ^{23}Na MAS NMR spectrum of P3-$Na_{2/3}Ni_{1/3}Mn_{2/3}O_2$ with only one site did not yield satisfactory results; at least three signals had to be included to produce an acceptable fit (Supporting Information Figure S2 and Table S1). Na^+ ion motion, if existent, should occur at similar time scales as in the P2 phase, given their similarity. Thus, the analysis of lineshapes suggests that there is a certain degree of structural disorder the P3 compared to the P2 polytype, which likely contributes to the large width of the XRD reflections in the former (Figure 1a). It is also supported by the notable differences in the width of the main ^{6}Li resonances between the two forms after Na/Li exchange (Figure 10). It is possible that disorder is triggered by both Ni/Mn exchange in the $\sqrt{3}a \times \sqrt{3}a$-type superlattice (in-plane disorder)[17] and the presence of stacking faults (interplane or registry disorder).[24] Interestingly, the P3 ^{23}Na NMR spectrum showed a small shoulder at shifts that match the P2 form, which could be explained by the existence of small regions of P2/P3 intergrowth[12] not detected by diffraction. This structural disorder could affect the efficiency of the hyperfine contact between Na and TM through bond distortions, resulting in the slightly lower center of gravity of the spectrum of P3- with respect to P2-$Na_{2/3}Ni_{1/3}Mn_{2/3}O_2$ (Figure 9).

While Na/Li exchange largely preserves the trends in ordering between phases at different compositions, subtle changes were still observed. The temperature at which the exchange occurred induced Li/Ni disorder in the layered structure of $Li_{0.9}Ni_{0.45}Mn_{0.55}O_2$. Structural disorder also appeared to increase during the transition from P2-$Na_{2/3}Ni_{1/3}Mn_{2/3}O_2$ to T2/O2-$Li_{2/3}Ni_{1/3}Mn_{2/3}O_2$, as implied by the presence of several small ^{6}Li NMR resonances above 600 ppm. In this case, the increase was likely the result of the formation of T2/O2 intergrowths or stacking faults, which, in turn, created new nonequivalent Li environments. Corresponding evidence of T2/O2/O3 intergrowth in O3-$Li_{2/3}Ni_{1/3}Mn_{2/3}O_2$ could not be obtained due to the existence of a significant low frequency tail in the 725 ppm ^{6}Li resonance (Figure 10). This main resonance is assigned to Li positions that are located in domains where high Ni/Mn ordering into a $\sqrt{3}a \times \sqrt{3}a$-type (honeycomb) pattern occurs. Such environments are similar to those found in the Li layers of $Li[Li_{1/3}Mn_{2/3}]O_2$ (Li_2MnO_3) because Li and Mn in the $[TMO_6]_\infty$ layer order following the same pattern.[27] The corresponding ^{6}Li MAS NMR signals were found to appear at shifts around 750−780 ppm, depending on the degree of stacking faults.[40] Going from O3-$Li[Li_{1/3}Mn_{2/3}]O_2$ to $Li_{2/3}[Ni_{1/3}Mn_{2/3}]O_2$ involves a replacement of Li by Ni in the $[TMO_6]_\infty$ layers, yet a small change in shift was seen between phases. Since Li^+ ions in the $[TMO_6]_\infty$ layers do not contribute to the hyperfine shift of the $[LiO_6]_\infty$ layers, the cationic substitution effectively results in the addition of four Li−O−Ni^{2+} "90°" (1st coordination shell) and two Li−O−Ni "180°" (2nd) hyperfine pathways for Li in the $[LiO_6]_\infty$ layers to the 8 Li−O−Mn^{4+} "90°" and 4 Li−O−Mn^{4+} "180°" pathways in $Li[Li_{1/3}Mn_{2/3}]O_2$.[38,48] The shift resulting from each Ni^{2+} in the first and second coordination shell is estimated to be −77 and 140 ppm, respectively, based on previous work.[38] Thus, the two Ni^{2+} contributions in each shell approximately cancel out.

CONCLUSIONS

Prismatic (P2 and P3) stackings were found for $Na_xNi_{x/2}Mn_{1-x/2}O_2$ when $x < 0.8$. At this value, transition to octahedral (O3) stacking takes place, most likely driven by the need to minimize Coulombic repulsions as cationic vacancies are occupied. This transition was accompanied by a discontinuity in unit cell dimensions that breaks the Vegard law. Further, a significant change in the degree of transition metal ordering in the respective layer was observed. While the O3 phases showed extensive disorder, considerable ordering was found for the P2 phases, although it may not be complete. The P3 phases constitute an intermediate case, in that they are considerably more ordered than O3, but some structural disorder, probably because of stacking faults or intergrowths, was obvious by NMR. The broad trends in intralayer ordering among polytypes were largely preserved after Na/Li exchange. However, the process induces Li/Ni exchange between layers, which likely increases the level of disorder with respect to the Na precursor, as well as a loss of registry between layers, leading to the formation of stacking faults, especially in the case of the P2 to T2/O2 transition. This observation is of importance if any of these materials are used as electrodes in Li-ion batteries, as these defects are known to result in barriers to Li diffusion in the structure.

ASSOCIATED CONTENT

Supporting Information

^{23}Na MAS NMR spectra of all phase pure $Na_xNi_{x/2}Mn_{1-x/2}O_2$; results of the simulation of the ^{23}Na MAS NMR spectra of $Na_{2/3}Ni_{1/3}Mn_{2/3}O_2$. This material is available free of charge via the Internet at http://pubs.acs.org.

AUTHOR INFORMATION

Corresponding Author

*E-mail: jcabana@uic.edu (J.C.); cpg27@cam.ac.uk (C.P.G.).

Present Address

Jie Xiao: Energy and Environment Directorate, Pacific Northwest National Laboratory, Richland, WA 99352

Notes

The authors declare no competing financial interest.

ACKNOWLEDGMENTS

This work was supported by the Assistant Secretary for Energy Efficiency and Renewable Energy, Office of Vehicle Tech-

nologies of the U.S. Department of Energy, under Contract DE-AC02-05CH11231, as part of the Batteries for Advanced Transportation Technologies (BATT) Program. The program is managed by LBNL for the Department of Energy. Binghamton and Stony Brook were supported under Subcontracts 6807148 and 6517749, respectively. J.C. is indebted to Generalitat de Catalunya (Spain) for a Beatriu de Pinós fellowship covering his work at Stony Brook. K.A.A. thanks the National Science Foundation for support via the Integrated Graduate Education and Research Training fellowship (Award No. 0549370).

REFERENCES

(1) Delmas, C.; Fouassier, C.; Hagenmuller, P. *Phys. B+C* **1980**, *99*, 81.
(2) Whittingham, M. S. *Chem. Rev.* **2004**, *104*, 4271.
(3) Delmas, C.; Braconnier, J. J.; Maazaz, A.; Hagenmuller, P. *Rev. Chim. Miner.* **1982**, *19*, 343.
(4) Brock, S. L.; Duan, N. G.; Tian, Z. R.; Giraldo, O.; Zhou, H.; Suib, S. L. *Chem. Mater.* **1998**, *10*, 2619.
(5) Post, J. E. *Proc. Natl. Acad. Sci. U. S. A.* **1999**, *96*, 3447.
(6) Kim, S.-W.; Seo, D.-H.; Ma, X.; Ceder, G.; Kang, K. *Adv. Energy Mater.* **2012**, *2*, 710.
(7) Terasaki, I.; Sasago, Y.; Uchinokura, K. *Phys. Rev. B* **1997**, *56*, No. R12685.
(8) Takada, K.; Sakurai, H.; Takayama-Muromachi, E.; Izumi, F.; Dilanian, R. A.; Sasaki, T. *Nature* **2003**, *422*, 53.
(9) Paulsen, J. M.; Thomas, C. L.; Dahn, J. R. *J. Electrochem. Soc.* **1999**, *146*, 3560.
(10) Paulsen, J. M.; Thomas, C. L.; Dahn, J. R. *J. Electrochem. Soc.* **2000**, *147*, 861.
(11) Kang, K.; Meng, Y. S.; Bréger, J.; Grey, C. P.; Ceder, G. *Science* **2006**, *311*, 977.
(12) Dollé, M.; Patoux, S.; Doeff, M. M. *Chem. Mater.* **2005**, *17*, 1036.
(13) Pasero, D.; Reeves, N.; Gillie, L.; Pralong, V.; West, A. R. *J. Electrochem. Soc.* **2007**, *154*, A760.
(14) Lu, Z. H.; Dahn, J. R. *J. Electrochem. Soc.* **2001**, *148*, A1225.
(15) Komaba, S.; Murata, W.; Ishikawa, T.; Yabuuchi, N.; Ozeki, T.; Nakayama, T.; Ogata, A.; Gotoh, K.; Fujiwara, K. *Adv. Funct. Mater.* **2011**, *21*, 3859.
(16) Paulsen, J. M.; Dahn, J. R. *Solid State Ionics* **1999**, *126*, 3.
(17) Paulsen, J. M.; Donaberger, R. A.; Dahn, J. R. *Chem. Mater.* **2000**, *12*, 2257.
(18) Roger, M.; Morris, D. J. P.; et al. *Nature* **2007**, *445*, 631.
(19) Guignard, M.; Didier, C.; Darriet, J.; Bordet, P.; Elkaim, E.; Delmas, C. *Nat. Mater.* **2013**, *12*, 74.
(20) MacKenzie, K. J. D.; Smith, M. E. *Multinuclear Solid-State Nuclear Magnetic Resonance of Inorganic Materials*; Pergamon Materials Series; Elsevier: Amsterdam, 2002.
(21) Grey, C. P.; Dupré, N. *Chem. Rev.* **2004**, *104*, 4493.
(22) Cabana, J.; Grey, C. P. In *Energy Production and Storage: Inorganic Chemical Strategies for a Warming World*; Crabtree, R. H., Ed.; John Wiley & Sons: West Sussex, U.K., 2010; pp 375.
(23) Laugier, J.; Bochu, B. *LMGP Suite of Programs for the interpretation of X-ray Experiments*; ENSP/Laboratoire des Materiaux et du Genie Physique: Saint Martin d'Heres, France. http://www.ccp14.ac.uk/tutorial/lmgp/celref.htm (Accessed July, 2013).
(24) Lu, Z.; Donaberger, R. A.; Dahn, J. R. *Chem. Mater.* **2000**, *12*, 3583.
(25) Bréger, J.; Kang, K.; Cabana, J.; Ceder, G.; Grey, C. P. *J. Mater. Chem.* **2007**, *17*, 3167.
(26) Shannon, R. D. *Acta Crystallogr.* **1976**, *A32*, 751.
(27) Strobel, P.; Lambert-Andron, B. *J. Solid State Chem.* **1988**, *75*, 90.
(28) Shin, Y. J.; Yi, M. Y. *Solid State Ionics* **2000**, *132*, 131.
(29) Goodenough, J. B. *Magnetism and the Chemical Bond*; Interscience Publishers: New York, 1963.
(30) Kanamori, J. *J. Phys. Chem. Solids* **1959**, *10*, 87.
(31) Chernova, N. A.; Nolis, G. M.; Omenya, F. O.; Zhou, H.; Li, Z.; Whittingham, M. S. *J. Mater. Chem.* **2011**, *21*, 9865.
(32) Shaju, K. M.; Ramanujachary, K. V.; Lofland, S. E.; Rao, G. V. S.; Chowdari, B. V. R. *J. Mater. Chem.* **2003**, *13*, 2633.
(33) Paulsen, J. M.; Dahn, J. R. *J. Electrochem. Soc.* **2000**, *147*, 2478.
(34) Lu, Z. H.; Dahn, J. R. *Chem. Mater.* **2001**, *13*, 2078.
(35) Paulsen, J. M.; Larcher, D.; Dahn, J. R. *J. Electrochem. Soc.* **2000**, *147*, 2862.
(36) Carlier, D.; Cheng, J. H.; Berthelot, R.; Guignard, M.; Yoncheva, M.; Stoyanova, R.; Hwang, B. J.; Delmas, C. *Dalton Trans.* **2011**, *40*, 9306.
(37) Aldi, K. A.; Cabana, J.; Sideris, P. J.; Grey, C. P. *Am. Mineral.* **2012**, *97*, 883.
(38) Zeng, D.; Cabana, J.; Bréger, J.; Yoon, W. S.; Grey, C. P. *Chem. Mater.* **2007**, *19*, 6277.
(39) Mustarelli, P.; Massarotti, V.; Bini, M.; Capsoni, D. *Phys. Rev. B* **1997**, *55*, 12018.
(40) Bréger, J.; Jiang, M.; Dupré, N.; Meng, Y. S.; Shao-Horn, Y.; Ceder, G.; Grey, C. P. *J. Solid State Chem.* **2005**, *178*, 2575.
(41) Yoon, W.-S.; Paik, Y.; Yang, X.-Q.; Balasubramanian, M.; McBreen, J.; Grey, C. P. *Electrochem. Solid State Lett.* **2002**, *5*, A263.
(42) Yoon, W. S.; Iannopollo, S.; Grey, C. P.; Carlier, D.; Gorman, J.; Reed, J.; Ceder, G. *Electrochem. Solid State Lett.* **2004**, *7*, A167.
(43) Bréger, J.; Dupré, N.; Chupas, P. J.; Lee, P. L.; Proffen, T.; Parise, J. B.; Grey, C. P. *J. Am. Chem. Soc.* **2005**, *127*, 7529.
(44) Hinuma, Y.; Meng, Y. S.; Kang, K. S.; Ceder, G. *Chem. Mater.* **2007**, *19*, 1790.
(45) Bréger, J.; Meng, Y. S.; Hinuma, Y.; Kumar, S.; Kang, K.; Shao-Horn, Y.; Ceder, G.; Grey, C. P. *Chem. Mater.* **2006**, *18*, 4768.
(46) Duer, M. J. *Introduction to Solid-State NMR Spectroscopy*; Blackwell Publishing, Inc.: Oxford, U.K., 2004.
(47) Han, O. H.; Jung, J. K.; Yi, M.-Y.; Kwak, J. H.; Shin, Y. J. *Solid State Commun.* **2000**, *117*, 65.
(48) Carlier, D.; Ménétrier, M.; Grey, C. P.; Delmas, C.; Ceder, G. *Phys. Rev. B* **2003**, *67*, No. 174103.1.